JOM, Vol. 72, No. 11, 2020
https://doi.org/10.1007/s11837-019-03970-2

Grain Refining Efficiency and the Role of Alloying Elements in Determining the Nucleation Potency of LaB_6 in Aluminum Alloys

LIJUN JING,[1] TAO LU,[1] and YE PAN[1,2]

1.—School of Materials Science and Engineering, Jiangsu Key Laboratory of Advanced Metallic Materials, Southeast University, Nanjing 211189, China. 2.—e-mail: panye@seu.edu.cn

This work discloses the refinement mechanism of LaB_6 in three binary aluminum alloys via grain refinement experiments, model calculation, and cooling curve analysis. The refining efficacy of LaB_6 in aluminum was influenced by an interfacial relationship which can be controlled by alloying with different solute elements. Al atoms attach directly onto the surface of the LaB_6 substrate during solidification. Because the lattice parameter of α-Al increased after alloying with larger metal atoms, the lattice mismatch between LaB_6 and Al matrix decreased. This investigation reveals that the nucleating behavior of LaB_6 can be influenced by adding solute Si, Mg, and Cu, and thereby offers a pathway for controlling the content of aluminum alloys.

INTRODUCTION

Grain refinement is a practical method to improve the mechanical properties and metallurgical quality of aluminum castings. In recent decades, much work has been focused on the mechanism of grain refinement in aluminum and its alloys.[1–4] A series of refinement theories have been proposed, such as the carbide/boride theory,[5] the phase diagram theory,[6] and the solute theory.[7,8] Although there are still some unaccountable results, it is generally accepted that both nucleant particles and solute elements contribute to the grain refinement phenomenon.[9,10] Hence, the characteristic of both nucleant particles and solute elements should be taken into consideration when investigating refinement phenomena.

According to traditional solute theory, the growth restriction factor, Q, is utilized to identify the effect of solute elements in aluminum on the final grains.[11–13] Easton et al.[12] indicated that Q was a measure of how rapidly the constitutionally undercooled zone was formed at the earliest stages of growth. It was found that grain size is related to solute content by a semi-empirical relationship:

$$d_{gs} = a + b/Q \tag{1}$$

where d_{gs} is the grain size, a is a constant related to the maximum number of particles that can be successfully activated as nucleants, b is another constant related to the nucleation potency of heterogeneous particles, and Q is the growth restriction factor which equals $mC_0(k-1)$.

StJohn et al.[14] developed the interdependence theory on the basis of Eq. 1. The interdependence theory links nucleant selection and grain growth together and assumes that grain formation is the result of the interdependence between nucleation and growth. StJohn indicated that Eq. 1 can be expressed as:

$$d_{gs} = x_{nfz} + x_{Sd} = 5.6\left(\frac{D \cdot z\Delta T_n}{v \cdot Q}\right) + x_{Sd} \tag{2}$$

where x_{nfz} represents a nucleation-free zone in which ΔT_{cs} is always less than $\Delta T_{n\text{-}min}$ for the most potent particles within the distribution described by $\Delta T_n - S_d$, D is the diffusion rate in the liquid, v is the growth velocity of the solid–liquid interface, ΔT_n is the undercooling for nucleation where the nucleation potency is proportional to $1/\Delta T_n$, and $z\Delta T_n$ is the incremental amount of undercooling required to re-establish $\Delta T_{n\text{-}min}$. According to Eq. 2, the value of constant a is equal to x_{Sd} and constant b is equal to

(Published online December 19, 2019)

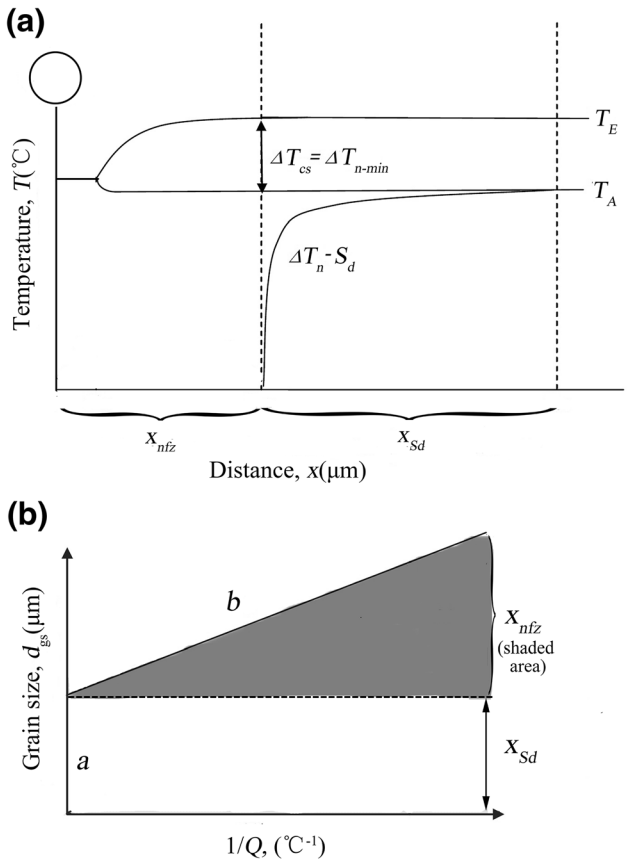

Fig. 1. (a) The two regions, x_{nfz} and x_{Sd}, establish the grain size of the microstructure; x_{nfz} represents a nucleation-free zone, where nucleation is not possible for the particle distribution described by $\Delta T_n - S_d$ (the $\Delta T_n - S_d$ curve is ΔT_n plotted against S_d for the range of particle diameters for values of $\Delta T_n < 0.8$°C, which are the particles most likely to become active nucleants); (b) the relationship between constants *a* and *b* and x_{nfz} and x_{Sd}.

$5.6 \cdot D \cdot z\Delta T_n/v$. Figure 1 clearly shows the two regions, i.e. x_{nfz} and x_{Sd}, establishing the final grain size and the relationship between Eqs. 1 and 2. The interdependence theory is able to clearly illustrate mechanisms of grain refinement, and provides directions for future research to improve the ability to accurately predict as-cast grain sizes. Wang Feng et al.[15] used this theory to analyze the effects of the peritectic elements, Ti, Zr, V, and Nb, and the eutectic elements, Cu, Mg and Si, on the refining effect of pure aluminum. Easton et al.[16] analyzed the refining behavior of an Al-Ti-B refiner in Al-Si alloys, suggesting that the addition of an Al-5Ti-1B refiner plays no role in Si poisoning.

Obviously, the influence of solute elements on grain size is not only attributed to the *Q* factor but also to the solid–liquid interface state during nucleation. Coudurier et al.[17] have shown that the solid–liquid interfacial composition plays a key role for a particular heterogeneous nucleating site to be effective. Zirconium and chromium are very different in size to aluminum, and the observed poisoning effects on the refinement efficacy of the Al-Ti-B master alloy also fits well with their theory. Paliwal et al.[18] investigated the variation of solid–liquid interfacial energy for Mg-Al binary alloys as a function of Al content. The calculated results reveal that the increasing Al content in Mg can significantly decrease the interfacial energy and the primary dendrite arm spacing. However, there are no sufficient experimental results to evidentially confirm this theory. It is also unclear how solute elements influence the interface state of two phases during solidification.

It has been demonstrated that Al_3Ti,[19] TiB_2,[1] and TiC[20] particles, etc. can refine the grain structures of aluminum alloys. LaB_6, as a favorable refiner in pure aluminum, has been developed due to its low lattice mismatch with Al.[21] Jing et al.[22] reported some specific crystalline orientation relationships between LaB_6 and Al. Li et al.[23] demonstrated that the morphology and dimensions of LaB_6 particles influenced its refining efficacy. However, the effects of solute elements on the refining efficacy of LaB_6 in Al-La-B refiner in aluminum alloys are still unclear. Investigation is required on the influence of various alloying elements in casting aluminum alloys on the refinement behavior of heterogeneous particles during solidification, taking advantage of the interdependence theory. Our previous works have indicated that LaB_6 can efficiently refine Al-Si alloys even with high content of silicon.[24,25] This means that a grain refiner including LaB_6 particles can be one of the most promising candidates for grain refinement application in cast Al-Si alloys. It is still undecided whether LaB_6 can yet show excellent grain-refining efficiency in cast Al-Mg and Al-Cu alloys. In particular, the rule that the refinement efficacy of LaB_6 is controlled by the interface matching behavior is not clear.

In the present work, the refining efficacy of LaB_6 particles was studied in Al-Si, Al-Mg and Al-Cu binary alloys. The influences of solute elements (Si, Mg, Cu) on the nucleation potency of LaB_6 have been discussed systematically based on the interdependence theory, considering an identical growth restriction factor. With analysis by x-ray diffraction (XRD) and high-resolution transmission electron microscopy (HRTEM), the rearrangement of atoms at the interface of LaB_6 and the Al matrix was identified, which was induced by the variation of the lattice parameter of Al with the solutions of different elements. The results indicate that it is more appropriate to take the lattice parameter of α-Al with alloying elements instead of pure Al when calculating the mismatch and studying the refinement mechanism.

EXPERIMENTAL PROCEDURE

Preparation of Alloys

The Al-2La-1B master alloy was fabricated by the melt reaction method at 900°C. The Al-Si, Al-Mg and Al-Cu alloys were prepared with high-purity aluminum (99.9 wt.% Al), Al-12Si alloy, pure

magnesium, and Al-50Cu alloy. The alloys were melted in a ceramic crucible in a 5-kW electrical resistance furnace to avoid impurities. Fifteen experimental alloys were designed to achieve a certain Q value, according to the data listed in Table I.[26] The Al-2La-1B master alloy was added into the melt at an addition level of 1.0 wt.% when the temperature was brought to 720 ± 5°C.

Measurement and Characterization

A cylindrical graphite mold (Φ 25 mm × 100 mm) surrounded by fire clay brick was used to evaluate the grain-refining performance of the grain refiners. The as-cast samples were sectioned 25 mm from the bottom surface. The samples were anodized in Barker's solution, and then examined with an optical microscope under polarized light. The grain sizes were measured by the linear intercept method (ASTM standard E112-96).

For thermal analysis, cylindrical graphite cups (Φ 20 mm × 5 mm wall thickness), were preheated in the melt, and filled by immersing them in the melt. Each cup was transferred to the cooling station and a K-type thermocouple quickly immersed into the center of the cup and 10 mm from the bottom of the cup, and then the temperatures were recorded by an AT4320 thermometrograph with an accuracy of ± 0.5°C.

The chemical compositions of the samples were analyzed with optical emission spectroscopy (see supplementary Table S1). For more obvious contrast and simplification of the experiments, the results of Al-1.0Si, Al-2.0 Mg and Al-2.1Cu were shown in grain refinement experiments and XRD analysis. The composition of the phases appearing in the master alloy and the variation of the lattice parameter of α-Al were characterized by XRD (D8-Discover; Bruker, Germany). When analyzing the phase composition of the master alloy, the test angle range was from 20° to 90°, the increment 0.02° and the scanning velocity 0.2 s/°. To compare the variation of the lattice parameters, the test angle range was from 30° to 40°, the increment 0.002° and scanning velocity 0.4 s/°. HRTEM analysis was utilized to investigate the interface state between LaB_6 and α-Al, which was performed on a JEM-2100F instrument. The samples for TEM analysis were fabricated by focused ion beam machine (Helios nanolab 600; FEI).

Table I. Data required for calculating the growth restriction factor, Q

	k_i	m_i	$m\ (k-1)$
Ti	7.8	33.3	220
Si	0.11	−6.6	5.9
Mg	0.51	−6.2	3.0
Cu	0.17	−3.4	2.8
La	0.00017	−1.8	1.8
B	0.23	−13.6	10.5

RESULTS AND DISCUSSION

Grain Refinement

Figure 2 shows the grain sizes of the three different binary alloys when Q = 6 K (in consideration of the trace addition level of the refiner and small residual solute elements, $Q = Q_{alloy}$). The mean grain sizes of the alloys without the addition of the Al-2La-1B refiner are all about 1350 μm, and are refined in various degrees with the addition of 1.0 wt.% of refiner. Specifically, the mean grain size of the Al-Si, Al-Mg and Al-Cu alloys are reduced to 393 μm, 195 μm, and 988 μm, respectively. Clearly, LaB_6 particles derived from the Al-2La-1B refiner perform a grain refinement effect in aluminum alloys. With addition of the Al-2La-1B refiner, a sufficient quantity of LaB_6 particles are uniformly distributed in the melt, providing more nucleation sites for α-Al during solidification, and thus favoring grain refinement. However, it is noticeable that, with the same refiner addition and the same value of the Q factor, the grain sizes of the three binary alloys are apparently different from each other (Fig. 2), suggesting they have different refining efficacies.

According to traditional solute theory, with the same value of the Q factor and refiner addition, the final grain size of aluminum alloys should be similar regardless of the alloying elements.[27] However, the grain sizes of the three binary alloys refined by LaB_6 show that there are obvious differences between them, although the Q factor is identical. Therefore, further work was undertaken to analyze this interesting phenomenon, which is in conflict with traditional solute theory.

Analysis with Interdependence Theory

The relationship between the grain size, d, and $1/Q$ of each alloy is in accordance with Eq. 1 under no refiner addition, as shown in Fig. 3. The constants b of each alloy are approximately identical (see supplementary Table S2), implying that the final grain size of the aluminum alloys is independent of the type of solute element. After adding the refiner, the grain size of each alloy is also related to the solute content by Eq. 1. However, the gradients of the d_{gs} versus $1/Q$ curves in each alloy with inoculation of LaB_6 are different, which is specifically $b_{uck} > b_{Si} > b_{Mg}$.

According to the XRD analysis of the Al-2La-1B refiner, basically there are only LaB_6 particles and no residual solute elements in the refiner (see supplementary Fig. S1). Figure 4 shows the morphology of the LaB_6 particles in the Al-La-B refiner. This confirms the dual-phase feature in the microstructures of the as-synthesized Al-2La-1B refiner, and that the particles distribute

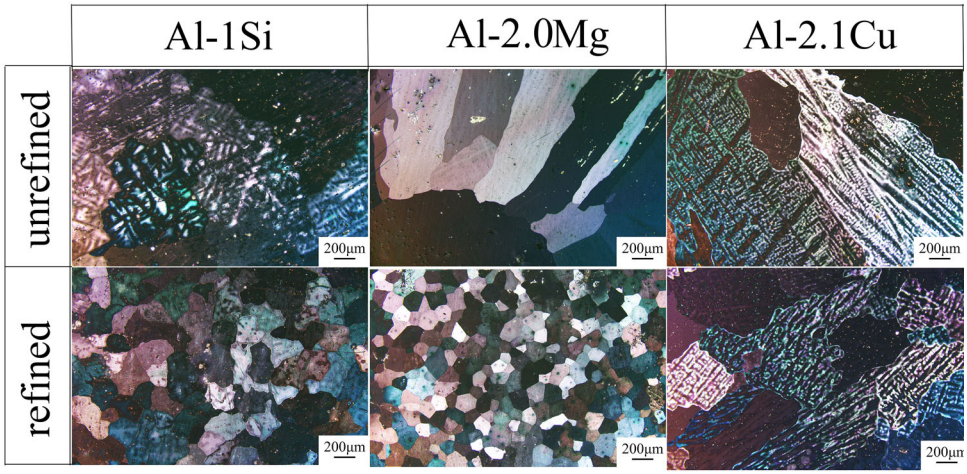

Fig. 2. Grain sizes of Al-1Si, Al-2.0 Mg and Al-2.1Cu alloys with and without refinement (Q = 6 K).

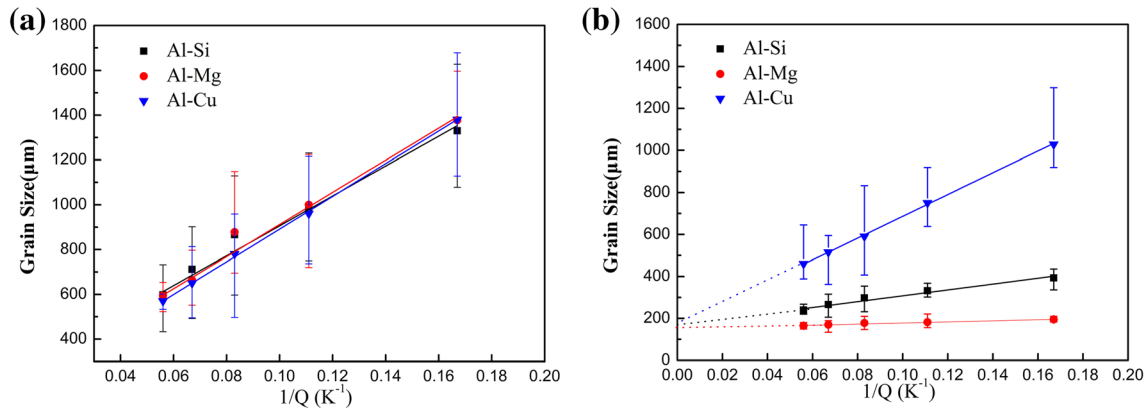

Fig. 3. Grain sizes of each binary aluminum alloy against the reciprocal of the growth restriction factor, Q: (a) without inoculation; (b) with inoculation.

homogenously in the Al matrix. Furthermore, the specific morphology of LaB_6 was found to be cubic-shaped, with a particle size of approximately 2 μm. Therefore, the influence of the intrinsic feature of the nucleant particles on the refinement efficacy is excluded. The diffusion rate, D, in the liquid is equal to 3.0×10^{-9} m^2/s because of the low content of solute elements.[10] On account of the identical pouring temperature and mold conditions, the cooling rate and temperature gradient remain identical, hence the growth velocity of the solid–liquid interface of each alloy can be regarded as the same. In conclusion, according to Eq. 2, the difference of the gradient of the grain size versus $1/Q$ is probably due to the different undercooling for nucleation ($\Delta T_{n,Cu} > \Delta T_{n,Mg}$).

The cooling curves of the three binary alloys with Q = 6 K are shown in Fig. 5, from which it can be seen that, after adding 1.0 wt.% of refiner, the undercooling for nucleation in each alloy is $\Delta T_{Cu} > \Delta T_{Si} > \Delta T_{Mg}$. This also indicates that the cooling rates of the three binary alloys during solidification are approximately the same. The results of the cooling curves indicate that the various refinement efficacies were because of the different undercooling for nucleation in each of the alloys.

XRD and HRTEM Analysis

Previous research indicated that the nucleation potency of heterogeneous substrates is decided by the lattice mismatch between the nucleant particles and Al.[28–30] The lattice mismatch between two phases is calculated by the following equation:[21]

$$\delta = \frac{|a_s - a_c|}{a_c} \times 100\% \qquad (3)$$

where δ is the lattice mismatch between the two phases, and a_s and a_c are the lattice parameters of LaB_6 and the Al matrix, respectively.

Previously, the lattice parameter of pure aluminum was used to calculate the lattice mismatch between the two phases.[21,31,32] However, much work[33–35] has shown that alloying elements indeed affect the lattice parameter of α-Al; e.g., adding a certain content of copper caused the lattice parameter of α-Al to decrease (see supplementary Table S3). Considering the fact that the primary

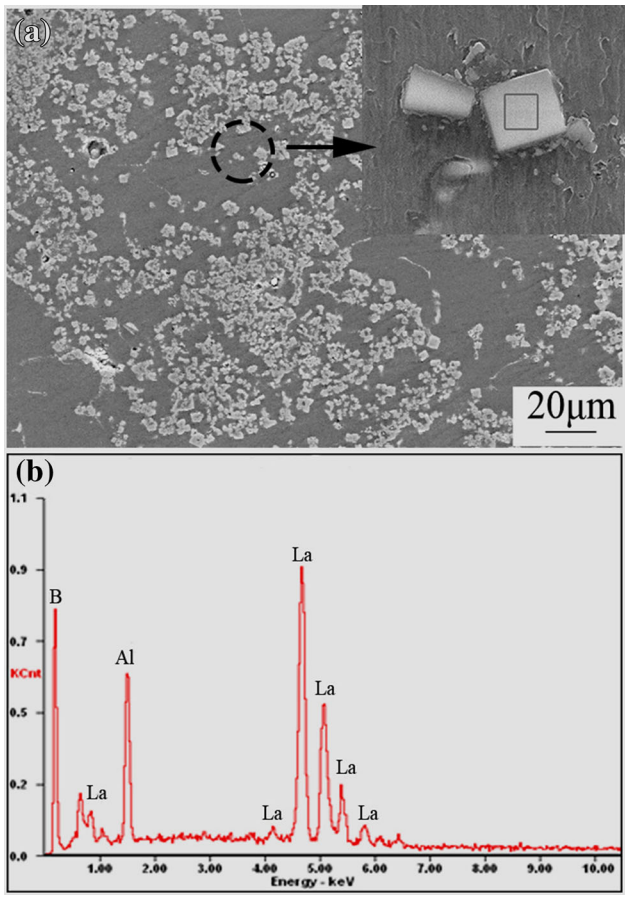

Fig. 4. SEM analysis: (a) the morphology of LaB_6 particles in the Al-2La-1B refiner; (b) EDS spectrum of LaB_6 particles.

phase in a common casting alloy is an alpha solid solution of aluminum instead of pure aluminum, it is reasonable to suppose that, owing to the different lattice parameters of α-Al resulting from various alloying elements, the lattice mismatch between LaB_6 and α-Al is not identical, and thus the nucleation potency of LaB_6 is also different in each alloy.

To demonstrate the above supposition, XRD analysis has been employed to compare the lattice parameters of pure Al, Al-1.0Si, Al-2.0 Mg and Al-2.1Cu, and the results are shown in Fig. 6, indicating that the <111> peak of α-Al in Al-2.0 Mg shifted to the left in comparison to pure aluminum, which means a certain enlargement of the lattice parameter, while the <111> peak of α-Al in Al-1.0Si alloy is very close to that in pure Al. This indicates that the addition of silicon in this content rarely affects the lattice parameter of α-Al. Remarkably, after adding the copper element, the lattice parameter becomes smaller for the right-shifting tendency of the <111> peak of α-Al. In consideration of Eq. 3, the certain decrease in the lattice parameter of α-Al in Al-2.1Cu alloy causes an inevitable increase in the lattice mismatch between LaB_6 and Al. This further reduces the nucleation potency of LaB_6, whereas the addition of a magnesium element shows the inverse tendency (see supplementary Table S3).

Figure 7 illustrates the interface state between LaB_6 and the Al matrix in the Al-2.0 Mg and Al-2.1Cu alloys. From Fig. 7a and b, two certain crystallographic orientation relationships between LaB_6 and the Al matrix can be found, namely, $(100)_{Al} \parallel (100)_{LaB6}$, $[001]_{Al} \parallel [001]_{LaB6}$ and $(110)_{Al} \parallel (110)_{LaB6}$, $[001]_{Al} \parallel [001]_{LaB6}$. It is clearly shown in Fig. 7c and e that Al nucleates directly onto the surface of the LaB_6 substrate during solidification. It is worth noting that, in the Al-2.0 Mg alloy, Al atoms arrange regularly at the interface between LaB_6 and the Al matrix, while in the Al-2.1Cu alloy, the Al atoms arrange irregularly in a couple layers at the interface. The atomic configuration of Al recovers from the irregular zones. An interpenetration area can also be seen at the interface, which may be due to substrate tuning (Fig. 7b).

After alloying with larger atoms, e.g., Mg, the lattice parameter of Al increases to a certain degree, such that the lattice mismatch between LaB_6 and Al decreases compared to that of pure aluminum. Aluminum atoms at the interface need little rearrangement during nucleation because of the small mismatch in the Al-Mg alloy. Inversely, in Al-2.1Cu alloys, the lattice parameter of the α-Al phase decreases after alloying with the smaller Cu atoms. The lattice mismatch between LaB_6 and Al decreases in the Al-2.1Cu alloy compared to that of pure aluminum. This leads to a rearrangement of aluminum atoms near the interface region and the interpenetration area, including expansion of the atomic spacing and even formation of dislocation. However, considering the irregular atomic arrangement is in a higher energy state than the regular atomic arrangement, more driving force is needed for aluminum to nucleate on the surface of LaB_6 in the Al-2.1Cu alloy than in the Al-2.0 Mg alloy.

In conclusion, it is believed that, due to the smaller mismatch resulting from alloying with an atom larger than aluminum, the more regular atomic configuration state at the interface leads to a higher nucleation potency of LaB_6 in Al-2.0 Mg than in Al-2.1Cu alloys.

The present work indicates that alloying elements in aluminum alloys will indeed influence the lattice parameters of α-Al to different degrees, leading to a variation of the lattice mismatch between LaB_6 and Al, which in turn affects the nucleation potency of LaB_6 in each of the binary alloys. A similar phenomenon has not been observed in the application of Al-Ti-B master alloys. It is possible that, when refining aluminum with the Al-Ti-B master alloy containing excess titanium, the TiB_2 particles act as the initial substrate, then a titanium-rich layer (presumed to be $TiAl_3$) will occur on the TiB_2 particles.[36,37] During solidification, the pre-existing α-Al, on which aluminum nucleats, forms by a peritectic reaction: $L + Al_3Ti \rightarrow$ α-Al. When

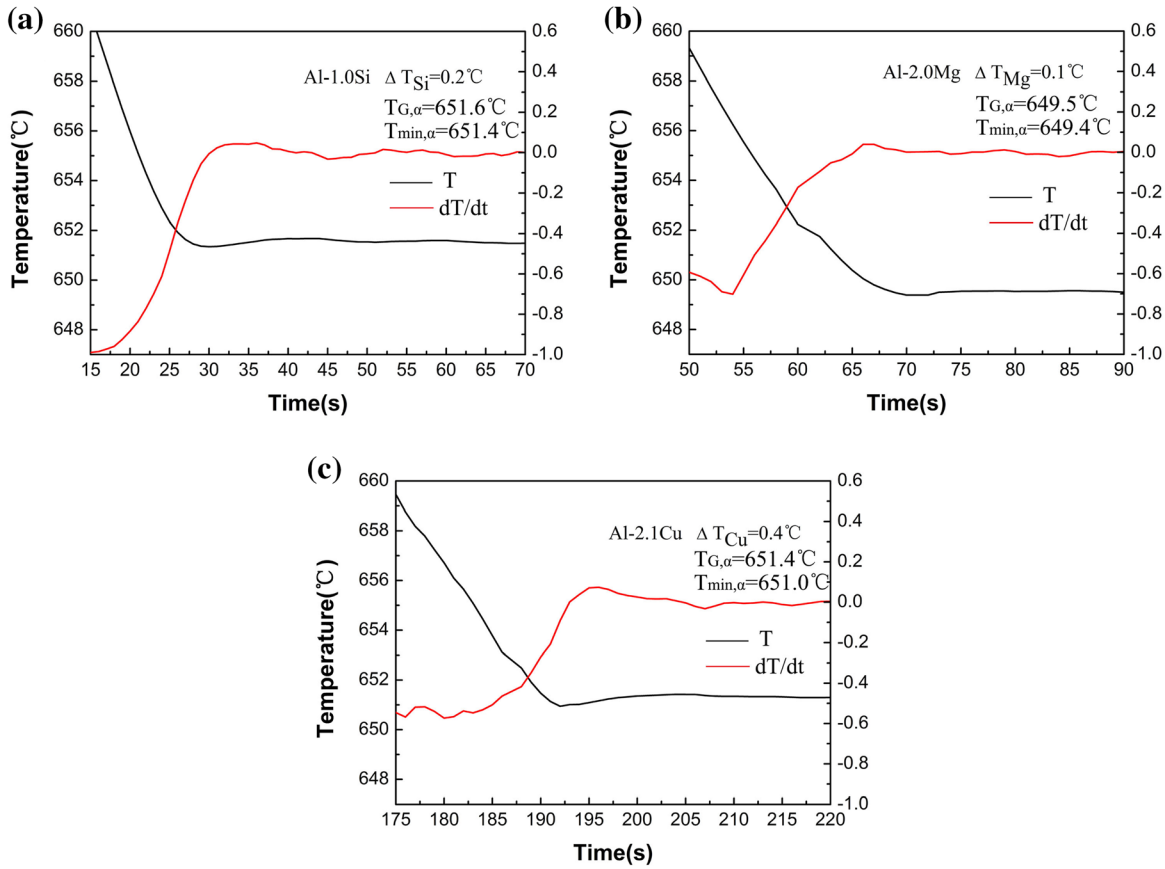

Fig. 5. Cooling curves of three binary alloys: (a) Al-1.0Si, (b) Al-2.0 Mg, and (c) Al-2.1Cu (Q = 6 K).

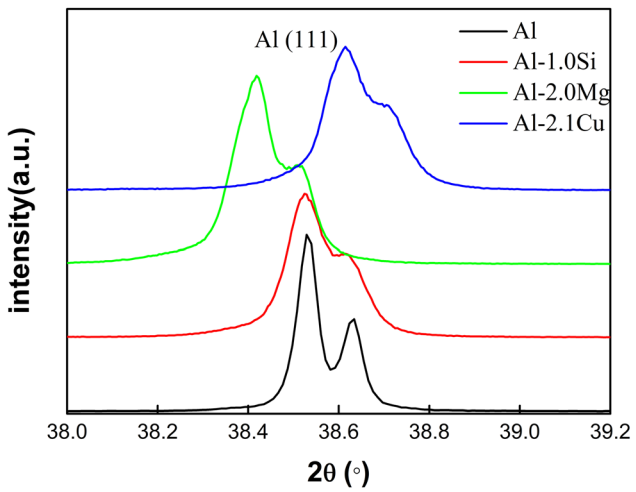

Fig. 6. XRD analysis: 111 diffraction peak of α-Al in pure Al, Al-1.0Si, Al-2.0 Mg and Al-2.1Cu.

refining aluminum by the Al-2La-1B refiner, LaB_6 is the active nuclei and aluminum nucleats directly onto it. The different nucleation state may result in the unusual refinement phenomenon between Al-La-B and Al-Ti-B refiners. This illustrates the atomic arrangement at the interface between Al and nucleation substrates (see supplementary Fig. S2). However, much more theoretical analysis and experimental proofs are needed to demonstrate the above suggestion.

CONCLUSION

1. The Al-La-B refiner can refine the grain structures of Al-Si, Al-Mg and Al-Cu alloys. However, the refiner shows different refining efficacy in each alloy, although the Q value is identical. Specifically, the refining efficiency of the Al-La-B refiner in Al-Mg alloys is the best while in Al-Cu alloys it is the worst.
2. According to the results of model calculation and cooling curves, the reason for the different refining efficiencies is due to the various nucleation potencies of the LaB_6 particles in each of the binary aluminum alloys.
3. XRD results demonstrate that the alloying elements in aluminum alloys will influence the lattice parameter of α-Al in different degrees. This leads to the variation of the lattice mismatch between LaB_6 and Al, and further affects the nucleation potency of activated LaB_6 particles in each binary alloy. The results of the HRTEM analysis also support this judgment. Due to the smaller mismatch resulting from alloying larger atoms than aluminum, the more

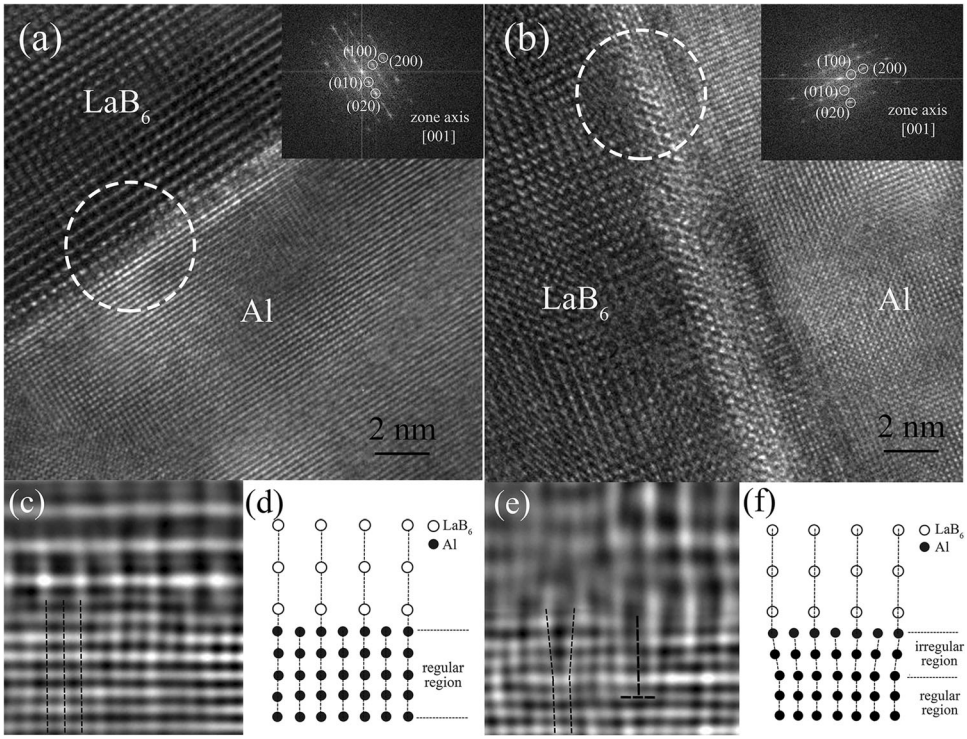

Fig. 7. HRTEM images showing the crystallographic interface between LaB_6 and the Al matrix in: (a) Al-2.0 Mg alloy and (b) Al-2.1Cu alloy; (c) and (e) are the inverse fast Fourier transformation images of the *marked local areas* in (a) and (b); (d) and (f) are schematics of the atomic arrangement near the interfaces of (c) and (e), respectively.

regular atomic configuration state at the interface leads to a higher nucleation potency of LaB_6 in Al-2.0 Mg than in Al-2.1Cu alloys.

ACKNOWLEDGEMENTS

This research is financially supported by Jiangsu key laboratory for advanced metallic materials (BM2007204) and the Opening Project of Jiangsu Key Laboratory of Advanced Structural Materials and Application Technology (ASMA201501). The authors thank Dr. K. Zhang and C.W Jin for their assistance with TEM analysis.

ELECTRONIC SUPPLEMENTARY MATERIAL

The online version of this article (https://doi.org/10.1007/s11837-019-03970-2) contains supplementary material, which is available to authorized users.

REFERENCES

1. Z.N. Chen, H.J. Kang, G.H. Fan, J.H. Li, Y.P. Lu, J.C. Jie, Y.B. Zhang, T.J. Li, X.G. Jian, and T.M. Wang, *Acta Mater.* 120, 168 (2016).
2. T.E. Quested and A.L. Greer, *Acta Mater.* 53, 4643 (2005).
3. A.L. Greer, P.S. Cooper, M.W. Meredith, W. Schneider, P. Schumacher, J.A. Spittle, and A. Tronche, *Adv. Eng. Mater.* 5, 81 (2003).
4. D.H. StJohn and M.A. Easton, *Alum. Cast House Technol.*, 151 (2001).
5. A. Cibula, *J. Inst. Met.* 76, 321 (1949).
6. F.A. Crossley and L.F. Mondolfo, *Trans. Am. Inst. Min. Metall. Pet. Eng.* 191, 1143 (1951).
7. M. Johnsson, L. Backerud, and G.K. Sigworth, *Metall. Mater. Trans. A* 24, 481 (1993).
8. I. Maxwell and A. Hellawell, *Acta Metall.* 23, 895 (1975).
9. M.A. Easton, M. Qian, A. Prasad, and D.H. StJohn, *Curr. Opin. Solid State Mater. Sci.* 20, 13 (2016).
10. D.H. StJohn, M. Qian, M.A. Easton, and P. Cao, *Acta Mater.* 59, 4907 (2011).
11. M.A. Easton and D.H. StJohn, *Light Met.*, 927 (2001).
12. M.A. Easton and D.H. StJohn, *Acta Mater.* 49, 1867 (2001).
13. M. Easton and D. StJohn, *Metall. Mater. Trans. A* 30, 1613 (1999).
14. D.H. Stjohn, M.A. Easton, M. Qian, and J.A. Taylor, *Metall. Mater. Trans. A* 44A, 2935 (2013).
15. F. Wang, Z. Liu, D. Qiu, J.A. Taylor, M.A. Easton, and M.X. Zhanga, *Acta Mater.* 61, 360 (2013).
16. M.A. Easton, A. Prasad, and D.H. StJohn, *Mater. Sci. Forum* 794, 161 (2014).
17. L. Coudurier, N. Eustathopoulos, P. Desre, and A. Passerone, *Acta Metall.* 26, 465 (1978).
18. Paliwal and I.-H. Jung, *Metall. Mater. Trans. A* 44, 1636 (2013).
19. G.K. Sigworth, *Metall. Mater. Trans. A* 15, 277 (1984).
20. P.T. Li, S.D. Liu, L.L. Zhang, and X.F. Liu, *Mater. Des.* 47, 522 (2013).
21. P.T. Li, W.J. Tian, D. Wang, and X.F. Liu, *J. Rare Earths* 30, 1172 (2012).
22. L. Jing, Y. Pan, T. Lu, and C. Li, *J. Mater. Eng. Perform.* 27, 1 (2018).
23. P.T. Li, C. Li, J.F. Nie, J. Ouyang, and X.F. Liu, *CrystEngComm* 15, 411 (2013).

24. Y. Chen, Y. Pan, T. Lu, S.W. Tao, and J.L. Wu, *Mater. Des.* 64, 423 (2014).
25. T. Lu, Y. Pan, J.L. Wu, S.W. Tao, and Y. Chen, *Int. J. Miner. Metall. Mat.* 22, 405 (2015).
26. A.M. Mitrasinovic and F.C.R. Hernandez, *Mater. Sci. Eng., A* 540, 63 (2012).
27. M. Easton and D. StJohn, *Metall. Mater. Trans. A* 36A, 1911 (2005).
28. M. Nowak, L. Bolzoni, and N.H. Babu, *Mater. Des.* 66, 366 (2015).
29. K. Kim, *Surf. Interface Anal.* 47, 429 (2015).
30. L. Bolzoni, M. Nowak, and N.H. Babu, *J. Alloys Compd.* 623, 79 (2015).
31. M.X. Zhang, P.M. Kelly, M.A. Easton, and J.A. Taylor, *Acta Mater.* 53, 1427 (2005).
32. S.Q. Liu, X. Wang, C.X. Cui, L.C. Zhao, S.J. Liu, and C. Chen, *Mater. Des.* 65, 432 (2015).
33. J. Wang, Y. Du, S.L. Shang, Z.K. Liu, and Y.W. Li, *J. Min. Metall. Sect. B-Metall.* 50, 37 (2014).
34. A. Tonejc and A. Bonefacic, *Scr. Metall.* 3, 145 (1969).
35. A. Tonejc and A. Bonefacic, *J. Appl. Phys.* 40, 419 (1969).
36. P. Schumacher, A.L. Greer, J. Worth, P.V. Evans, M.A. Kearns, P. Fisher, and A.H. Green, *Mater. Sci. Technol.* 14, 394 (1998).
37. Z. Fan, Y. Wang, Y. Zhang, T. Qin, X.R. Zhou, G.E. Thompson, T. Pennycook, and T. Hashimoto, *Acta Mater.* 84, 292 (2015).